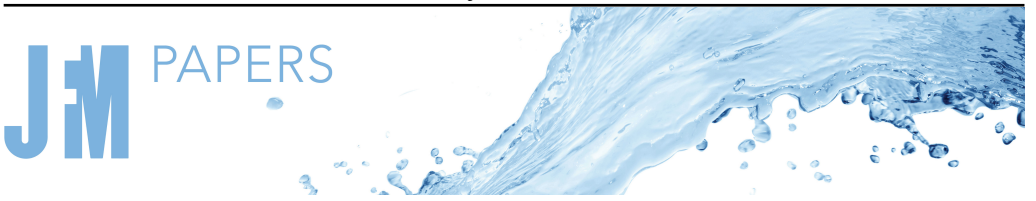
J. Fluid Mech. (2026), *vol.* 1042, A43, doi:10.1017/jfm.2026.12016



Note on flow structure near the corner of a wedge

H.K. Moffatt[1]

[1]Department of Applied Mathematics and Theoretical Physics, Wilberforce Road, Cambridge CB3 0WA, UK

Corresponding author: H.K. Moffatt, hkm2@cam.ac.uk

(Received 14 April 2026 UTC; revised 27 June 2026 UTC; accepted 5 August 2026 UTC)

The low-Reynolds-number flow near the sharp corner of a wedge-shaped obstacle is reconsidered. For flow round the corner, the velocity is zero (and the vorticity infinite) at the vertex, yet it is shown that fluid particles accelerate as their distance r from the vertex decreases, i.e. as they approach the point of zero velocity. By contrast, for symmetric flow towards the corner, fluid particles decelerate as the corner region is approached. The limiting case in which the wedge collapses to a flat plate is given special consideration. For flow round the edge of the plate (with symmetric streamfunction), the streamlines are parabolic. In this flat-plate limit, a family of asymmetric flows is determined.

Key words: low-Reynolds-number flows

1. Introduction

The low-Reynolds-number flow in a corner bounded by fixed planes $\theta = \pm\alpha$ was considered by Moffatt (1964). It had been shown by Dean & Montagnon (1949) that if the angle 2α of the corner is less than a critical value $2\alpha_m \approx 147^o$, the velocity is proportional to a complex power of distance r from the corner. I showed that this implies the existence of an infinite self-similar sequence of eddies as the corner is approached. This phenomenon was quite unexpected at the time, and it was natural that attention should be focused on it. These corner eddies were observed experimentally in a range of geometries by Taneda (1979), and have since been observed in many situations of practical importance. A book has been devoted to the phenomenon (Shankar 2007).

Much less attention has been devoted to the situation when the angle 2α is reflex, i.e. greater than π. In this case, on which we focus in this note (which may be regarded as a somewhat belated appendix to Moffatt 1964), we are dealing with two-dimensional flow near the vertex (alternatively described as the 'corner' or 'tip') of a wedge of interior

© The Author(s), 2026. Published by Cambridge University Press. This is an Open Access article, distributed under the terms of the Creative Commons Attribution licence (https://creativecommons.org/licenses/by/4.0/), which permits unrestricted re-use, distribution and reproduction, provided the original article is properly cited.

https://doi.org/10.1017/jfm.2026.12016 Published online by Cambridge University Press

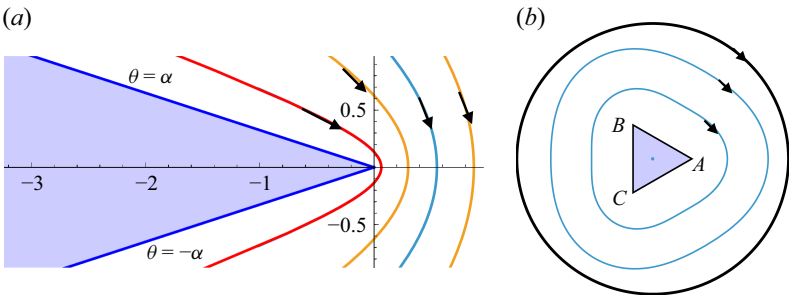


Figure 1. (*a*) Flow round a corner between fixed planes $\theta = \pm\alpha$ with $\pi/2 < \alpha \leq \pi$; (*b*) schematic of flow around a cylinder of triangular cross-section driven by rotation of an outer circular cylinder; in this note, we are concerned only with the flow near the vertices A, B or C of the inner cylinder.

angle $2\pi - 2\alpha < \pi$. The streamfunction $\psi(r, \theta)$ may be either an even function of θ (flow round the corner), or an odd function (flow towards or away from the corner), and in the Stokes flow situation, the general flow is a linear combination of these flows, which may be considered separately.

We note that the Wolfram demonstration 'flow round a corner' (Bradley 2015) is concerned only with an inviscid fluid and solutions of Laplace's equation $\nabla^2\psi = 0$ in corner geometries. The behaviour may be contrasted with the behaviour of a viscous fluid described by the biharmonic equation $\nabla^4\psi = 0$ coupled with no-slip boundary conditions, as described in the present note. The situations are quite distinct in that, for flow round the corner, the velocity is infinite at the tip in the inviscid situation, but zero at the tip in the viscous situation (although the vorticity is infinite). Moreover, for acute-angled corners, eddies do not occur for inviscid fluids, and are solely due to the influence of viscosity.

2. Stokes solution: a recapitulation

Consider first the two-dimensional flow round a sharp corner (i.e. one of zero radius of curvature) formed by two fixed planes $\theta = \pm\alpha$ with $\pi/2 < \alpha \leq \pi$, on which the no-slip condition is imposed. The situation is illustrated in figure 1(*a*). At the origin $r = 0$, the velocity $\boldsymbol{u} = (u_r, u_\theta)$ is zero, and we may therefore assume that the local Reynolds number based on distance r from the corner is small, and fluid inertia is negligible. It is supposed that the flow is driven by some mechanism far from the corner. (Figure 1*b* illustrates one possible example: this is Couette flow between two cylinders, with the inner cylinder of triangular cross-section fixed, and the flow being driven by rotation of the outer circular cylinder. Of course any inner cylinder of polygonal cross-section with interior angles less than π would present similar problems. We are concerned here only with the flow in the immediate vicinity of any vertex of the inner cylinder.) For the situation considered here, with the angle 2α in the reflex range $\pi \leq 2\alpha \leq 2\pi$, the streamfunction $\psi(r, \theta)$ has the asymptotic form

$$\psi(r, \theta) \sim r^{\mu+1} f(\theta, \alpha) \quad \text{as} \quad r \to 0, \tag{2.1}$$

where the exponent μ depends on the angle α in a manner that must be determined. The velocity $\boldsymbol{u} = (u_r, u_\theta)$ is then given by

$$u_r = r^{-1}\partial\psi/\partial\theta = r^\mu \partial f/\partial\theta, \qquad u_\theta = -\partial\psi/\partial r = -(\mu+1)r^\mu f(\theta, \alpha). \tag{2.2}$$

https://doi.org/10.1017/jfm.2026.12016 Published online by Cambridge University Press

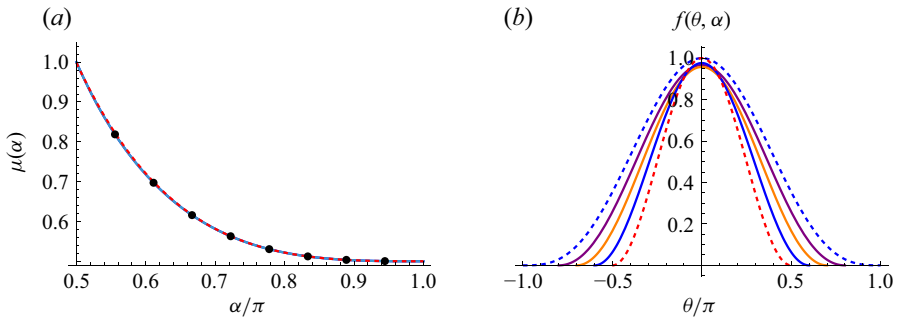


Figure 2. (*a*) The function $\mu(\alpha)$ over the range $1/2 \le \alpha/\pi \le 1$ (continuous blue curve); the red, dashed curve superposed on this is the three-term asymptotic function $\mu_a(\alpha)$ (2.10); the black points are as obtained by a graphical method by Dean & Montagnon (1949). (*b*) The function $f(\theta, \alpha)$, given by (2.8), for $\alpha/\pi = 0.5$ (red, dashed), 0.6 (blue), 0.7 (orange), 0.8 (purple) and 1 (blue, dashed).

For the case in which u_r is antisymmetric about the bisector $\theta = 0$ (as in figure 1*a*), $f(\theta, \alpha)$ is an even function of θ, and is given by

$$f(\theta, \alpha) = A\cos(\mu+1)\theta + B\cos(\mu-1)\theta. \tag{2.3}$$

Here, the scaling is arbitrary, and so the coefficient A, say, is arbitrary (being in principle determined by the remote forcing conditions, here unspecified). The no-slip conditions are satisfied on $\theta = \pm\alpha$ provided

$$A\cos(\mu+1)\alpha + B\cos(\mu-1)\alpha = 0, \tag{2.4}$$

and

$$A(\mu+1)\sin(\mu+1)\alpha + B(\mu-1)\sin(\mu-1)\alpha = 0. \tag{2.5}$$

For a non-trivial solution for B/A, μ must then satisfy the transcendental equation

$$F(\alpha, \mu) \equiv \sin 2\mu\alpha + \mu \sin 2\alpha = 0, \tag{2.6}$$

and the condition of zero velocity at $r = 0$ requires that $\mu > 0$. When $\alpha = \pi/2$, $\sin\pi\mu = 0$, and the smallest positive root is $\mu = 1$. For $\alpha > \pi/2$, with $\mu = \mu(\alpha)$ determined as the smallest real positive root of (2.6), and with the convenient choice

$$A = \frac{\cos[(\mu-1)\alpha]}{2\sin\alpha} \tag{2.7}$$

for the pre-factor A, (2.3) then gives

$$f(\theta, \alpha) = \sin\alpha\mu\cos\theta\cos\mu\theta - \cot\alpha\cos\alpha\mu\sin\theta\sin\mu\theta, \tag{2.8}$$

which remains bounded for all $\alpha \in [\pi/2, \pi]$. Figure 2(*a*) shows the function $\mu(\alpha)$, obtained as the zero contour of the function $F(\alpha, \mu)$ starting from the point $\alpha = \pi/2$, $\mu = 1$. Note that since $\mathrm{d}F = (\partial F/\partial\alpha)\mathrm{d}\alpha + (\partial F/\partial\mu)\mathrm{d}\mu = 0$, it follows that

$$\frac{\mathrm{d}\mu}{\mathrm{d}\alpha} = -\frac{\partial F/\partial\alpha}{\partial F/\partial\mu} = -\frac{2\mu(\cos 2\alpha\mu + \cos 2\alpha)}{2\alpha\cos 2\alpha\mu + \sin 2\alpha}, \tag{2.9}$$

and so the curve of figure 2(*a*) may be obtained alternatively by numerical integration of (2.9) with starting condition $\mu(\pi/2) = 1$. Either way, the resulting function $\mu(\alpha)$ in figure 2(*a*) evidently decreases monotonically from 1 to 1/2 as α increases from $\pi/2$ to π. The vorticity $\omega = -\nabla^2\psi$ is proportional to $r^{\mu-1}$, and is therefore singular at the vertex

https://doi.org/10.1017/jfm.2026.12016 Published online by Cambridge University Press

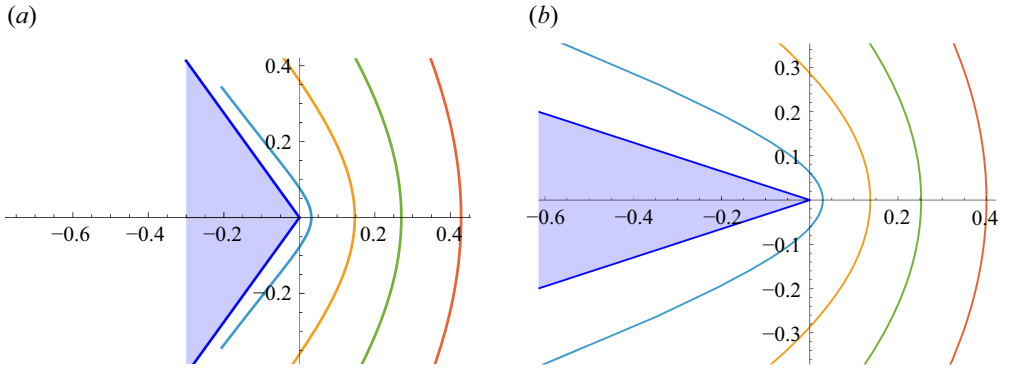


Figure 3. Streamlines $\psi(r,\theta) = r^{\mu(\alpha)+1} f(\theta,\alpha) =$ const. for (*a*) $\alpha = 0.7\pi$ and (*b*) $\alpha = 0.9\pi$. Note how, in both cases, the streamlines converge with decreasing distance from the vertex. Arrows on the streamlines are not included, since Stokes flows, with negligible inertia, are reversible.

$r = 0$ for all $\alpha > \pi/2$. Analysis of (2.6) reveals the asymptotic form as $\alpha \to \pi$

$$\mu(\alpha) \sim \mu_a(\alpha) + \mathrm{O}(\pi-\alpha)^6, \quad \text{where} \quad \mu_a(\alpha) = \frac{1}{2} + \frac{(\pi-\alpha)^3}{4\pi} + \frac{(\pi-\alpha)^5}{16\pi}. \tag{2.10}$$

The three-term asymptotic function $\mu_a(\alpha)$ is superposed (red, dashed) on $\mu(\alpha)$ in figure 2(*a*) and is fortuitously accurate over the whole range $1/2 \le \alpha/\pi \le 1$ (even at the lower limit, where $\mu_a(\pi/2) \approx 0.9987$). The black dots on this curve are at points obtained by Dean & Montagnon (1949) by a graphical procedure, and are also accurate to three significant figures, a fine achievement in the pre-computer age!

The function $f(\theta,\alpha)$ (as given by (2.8)) is plotted in figure 2(*b*) for several values of α. In the limiting case $\alpha = \pi/2$, $f(\theta,\pi/2) = \cos^2\theta$ (the red dashed curve in figure 2*b*), and the flow is simply a uniform shear parallel to the plane boundary $x\ (= r\cos\theta) = 0$.

The other limiting case $\alpha = \pi$ in which the 'wedge' of figure 1(*a*) collapses to a flat plat on $\theta = \pm\pi$, requires special consideration. In this case, with $\alpha = \pi$ and $\mu = 1/2$, equation (2.4) is identically satisfied, and (2.5) gives

$$-(3/2)A + (1/2)B = 0. \tag{2.11}$$

Hence, taking $A = 1/4$ (the limit of (2.7) as $\alpha \to \pi$), equation (2.8) gives

$$f(\theta,\pi) = \frac{1}{4}[\cos(3\theta/2) + 3\cos(\theta/2)] = \cos^3(\theta/2). \tag{2.12}$$

This is the blue dashed curve in figure 2(*b*).

2.1. *Flow structure*

We can now plot the streamlines $\psi(r,\theta) = r^{\mu(\alpha)+1} f(\theta,\alpha) =$ const. Two examples are shown in figure 3, for $\alpha = 0.7\pi$ and $\alpha = 0.9\pi$.

In the limiting case $\alpha = \pi$, the streamfunction is given by

$$\psi(r,\theta) = r^{3/2}\cos^3(\theta/2) = \left[r\cos^2(\theta/2)\right]^{3/2} = \left[\frac{1}{2}r(1+\cos\theta)\right]^{3/2}. \tag{2.13}$$

Hence, with $x = r\cos\theta$, the streamline $\psi = \psi_0$ (const.) is the parabola

$$r + x = 2\psi_0^{2/3} = 2a, \ \text{ say}, \tag{2.14}$$

https://doi.org/10.1017/jfm.2026.12016 Published online by Cambridge University Press

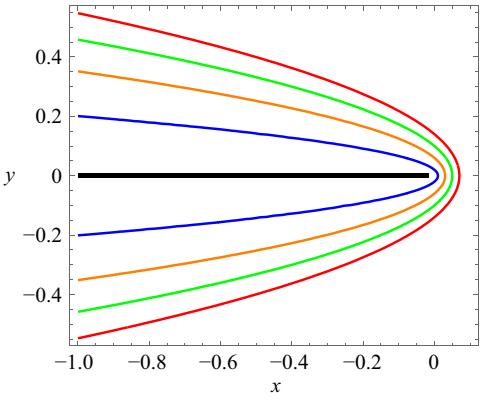


Figure 4. Parabolic streamlines in the flat-plate limit $\alpha = \pi$, with $\psi(r, \theta) = [(1/2)r(1 + \cos\theta)]^{3/2}$.

or equivalently

$$y^2 = 4a(a - x). \tag{2.15}$$

The family of parabolic streamlines (for varying a) is shown in figure 4.

2.2. *Acceleration along streamlines as the corner region is approached*

It is evident from figures 3 and 4 that the streamlines invariably converge when approaching the corner, indicating acceleration with decreasing distance from the vertex $r = 0$. At first sight, this appears paradoxical as the velocity $|\boldsymbol{u}|$ is proportional to $r^{\mu(\alpha)}$ which tends to zero for all α in the range $\pi/2 < \alpha \leq \pi$. It is a situation in which we apparently have fluid particles accelerating with decreasing distance from the stagnation point at the vertex! In this respect, the sketch of figure 4(a) of Moffatt (1964) is, however, misleading; we take the opportunity to correct this here.

The paradox arises because, although the decrease of velocity to zero occurs on radial lines $\theta = \text{const.}$, it does not do so on streamlines as may be shown as follows. From (2.2), we have

$$|\boldsymbol{u}| = \left[u_r^2 + u_\theta^2\right]^{1/2} = r^{\mu(\alpha)}\left[(\partial f/\partial\theta)^2 + (\mu+1)^2 f^2(\theta, \alpha)\right]^{1/2}. \tag{2.16}$$

We may evaluate this on any streamline $\psi = \psi_0$, on which $r = [\psi_0/f(\theta, \alpha)]^{1/(1+\mu(\alpha))}$. On such a streamline

$$|\boldsymbol{u}(\theta, \alpha)| = c\left[(\partial f/\partial\theta)^2 + (\mu+1)^2 f^2(\theta, \alpha)\right]^{1/2} f(\theta, \alpha)^{-\mu(\alpha)/[1+\mu(\alpha)]}, \tag{2.17}$$

where $c = \psi_0^{\mu(\alpha)/[\mu(\alpha)+1]}$. The expression $c^{-1}|\boldsymbol{u}(\theta, \alpha)|$ is plotted in figure 5 for $0 < \theta < \pi/2$, for various values of α. As expected, in every case, the speed increases as θ decreases towards zero, so that any fluid particle does indeed accelerate as its distance r from the vertex decreases. The dependence of $|\boldsymbol{u}|$ on θ in (2.16) evidently more than compensates the decrease due to the factor $r^{\mu(\alpha)}$. (In the limiting case $\alpha = \pi$ with $\mu = 1/2$, the expression (2.17) evaluates explicitly to the function $(3/2^{5/6})\sqrt{1 + \cos\theta}$, monotonic over the range $0 < \theta < \pi$.)

3. Flow symmetric about $\theta = 0$

Consider now the complementary situation of flow symmetric about $\theta = 0$, as shown in figure 8(a,b) below. This is again a Stokes flow, and the flow can be either towards or away

https://doi.org/10.1017/jfm.2026.12016 Published online by Cambridge University Press

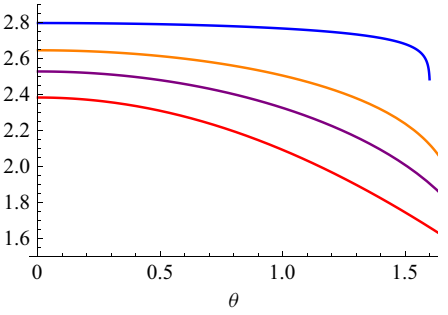


Figure 5. The behaviour of $c^{-1}|\boldsymbol{u}(\theta, \alpha)|$ on any streamline $\psi = \psi_0$ over the range $0 < \theta < \pi/2$, for $\alpha = 0.51\,\pi$ (blue), $0.56\,\pi$ (orange), $0.60\,\pi$ (purple) and π (red). In every case, the curves are monotonically increasing as θ decreases towards 0.

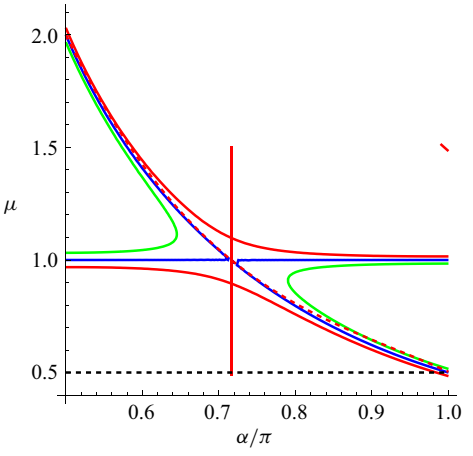


Figure 6. Contour $G(\alpha, \mu) = 0$ (blue) for $\pi/2 \le \alpha \le \pi$; the (dashed, red) curve $\mu = \mu_a(\alpha)$ given by (3.3) is superposed, indicating reasonable coincidence over the full range. Also shown are the contours $G(\alpha, \mu) = -0.1$ (green) and $+0.1$ (red). The zero contour crosses the line $\mu = 1$ at $\alpha = \alpha_c$ as indicated by the red vertical line; α_c is the root of $\tan 2\alpha = 2\alpha$ in this range, i.e. $2\alpha_c \approx 1.43\pi \approx 257^o$.

from the vertex of the wedge. An important example is the flow (relative to the body) near the leading edge of any sharp-tipped cylindrical body moving into a fluid at rest 'at infinity'. The local streamfunction is now antisymmetric in θ and has the form

$$\psi(r, \theta) \sim r^{\mu+1} g(\theta, \alpha) = r^{\mu+1}[C \sin(\mu + 1)\theta + D \sin(\mu - 1)\theta], \tag{3.1}$$

and the no-slip conditions on $\theta = \pm\alpha$ are now satisfied provided

$$G(\alpha, \mu) \equiv \sin 2\mu\alpha - \mu \sin 2\alpha = 0. \tag{3.2}$$

Note first that this is identically satisfied for all α if $\mu = 1$; however, equation (3.1) then gives $g(\theta, \alpha) = C \sin 2\theta$, and the no-slip conditions can be satisfied only if $C = 0$. The possibility $\mu = 1$ thus yields only the trivial solution, and can be safely ignored (but see below).

From (3.2), when $\alpha = \pi/2$, $\sin \pi\mu = 0$, so the next possibility with $\mu > 0$ is $\mu = 2$. The contour $G(\alpha, \mu) = 0$ starting from the point $\alpha = \pi/2,\ \mu = 2$ is shown in figure 6. The required function $\mu(\alpha)$ is given by the curved part of this contour, which crosses the line $\mu = 1$ at $\alpha = \alpha_c$ (indicated by the vertical red line); the 'critical angle' is $\alpha_c \approx 0.175\pi$,

https://doi.org/10.1017/jfm.2026.12016 Published online by Cambridge University Press

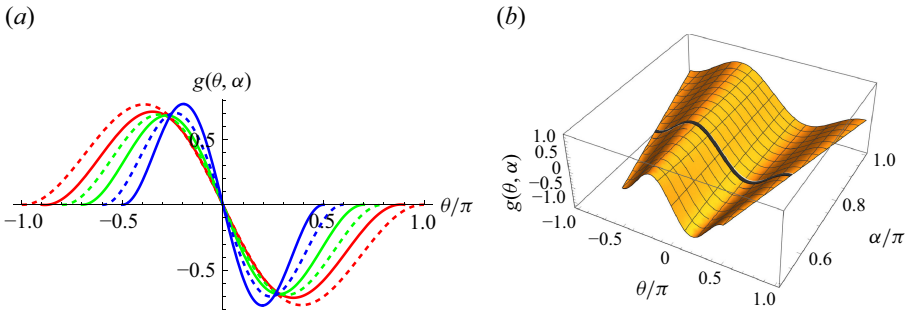


Figure 7. (*a*) The function $g(\theta,\ \alpha)$, given by (3.5), over the range $\alpha \le \theta \le \alpha$ for $\alpha/\pi = 0.5$ (blue), 0.6 (blue, dashed), 0.7 (green), 0.8 (green, dashed), 0.9 (red) and 1 (red, dashed); (*b*) three-dimensional plot of the same function over the range $\{\pi/2 < \alpha < \pi,\ -\alpha < \theta < \alpha\}$; note that the function $g(\theta,\ \alpha)$ extends continuously over the gap at $\alpha = \alpha_c \approx 0.715\pi$, where the quotient (3.5) is indeterminate; the blue curve on this plot, given by (3.6), fills the 'criticality' gap $0.71 < \alpha/\pi < 0.72$.

as determined in the following paragraph. We include also the contours $G(\alpha,\ \mu) = -0.1$ (green) and $+0.1$ (red) to indicate the structure near the critical point $\{\mu = 1,\ \alpha = \alpha_c\}$. We have also superposed on the zero contour the red dashed curve (obtained by simple curve fitting)

$$\mu = \mu_a(\alpha) = 2 - 2.21(\alpha - \pi/2) + 1.303(\alpha - \pi/2)^2 - 0.32(\alpha - \pi/2)^3, \tag{3.3}$$

which evidently provides a reasonable approximation over the whole range $\pi/2 \le \alpha \le \pi$. In particular, $\mu_a(\alpha_c) = 1.00$.

Just as for equation (2.9) above, we now have for the symmetric case

$$\frac{\mathrm{d}\mu}{\mathrm{d}\alpha} = -\frac{\partial G/\partial\alpha}{\partial G/\partial\mu} = -\frac{2\mu(\cos 2\mu\alpha - \cos 2\alpha)}{2\alpha\cos 2\mu\alpha - \sin 2\alpha}. \tag{3.4}$$

Here, obviously the numerator $\partial G/\partial\alpha = 0$ on $\mu = 1$. Also, the denominator $\partial G/\partial\mu = 2\alpha\cos 2\mu\alpha - \sin 2\alpha$ vanishes on the line $\mu = 1$ where $\tan 2\alpha = 2\alpha$, i.e. at $\alpha = \alpha_c \approx 2.247 = 0.715\pi$, or equivalently $2\alpha_c \approx 257^o$. Hence the expression (3.4) for $\mathrm{d}\mu/\mathrm{d}\alpha$ is indeterminate at the critical point $\{\alpha = \alpha_c,\ \mu = 1\}$. The angle α_c has been previously recognised by Moffatt & Duffy 1980 as the angle at which, in the context of flow driven by hinged plates in relative angular motion, a changeover occurs in the behaviour near the corner from that described by a local similarity solution $\psi \sim r^2$ when $\alpha < \alpha_c$ to that determined by remote conditions and described by the leading term of an asymptotic expansion $\psi \sim r^{\mu(\alpha)+1}$ when $\alpha > \alpha_c$.

With $\mu(\alpha)$ determined, and $D = -C\sin[\alpha(\mu(\alpha)+1)]\csc[\alpha(\mu(\alpha)-1)]$, the function $g(\theta, \alpha)$ in (3.1) may now be obtained. Choosing $C = -1/(2\sin\alpha)$, (cf. the freedom of choice for $A(\alpha)$ in (2.7)), we find

$$g(\theta, \alpha) = \frac{\cos[\alpha\ \mu(\alpha)]\cos\theta\sin[\theta\ \mu(\alpha)] - \cot\alpha\sin[\alpha\ \mu(\alpha)]\sin\theta\cos[\theta\ \mu(\alpha)]}{\sin[\alpha(\mu(\alpha)-1]}. \tag{3.5}$$

The numerator in this expression is identically zero (for all θ) when $\mu(\alpha) = 1$, i.e. when $\alpha = \alpha_c$. This is, however, compensated by the zero of the denominator at $\mu(\alpha) = 1$. Adopting the approximation (3.3), $\mu(\alpha) \approx \mu_a(\alpha)$, the function (3.5) has been plotted over the range $-\alpha \le \theta \le \alpha$, as shown in figure 7(*a*) for $\alpha/\pi = 0.5, 0.6, 0.7, 0.8, 0.9, 1$. The three-dimensional plot of figure 7(*b*) shows that this family of curves passes smoothly through the critical point at $\alpha = \alpha_c \approx 0.715\pi$. The blue curve on this plot fills the 'criticality' gap $0.71 < \alpha/\pi < 0.72$ and is given to good approximation by the equation

https://doi.org/10.1017/jfm.2026.12016 Published online by Cambridge University Press

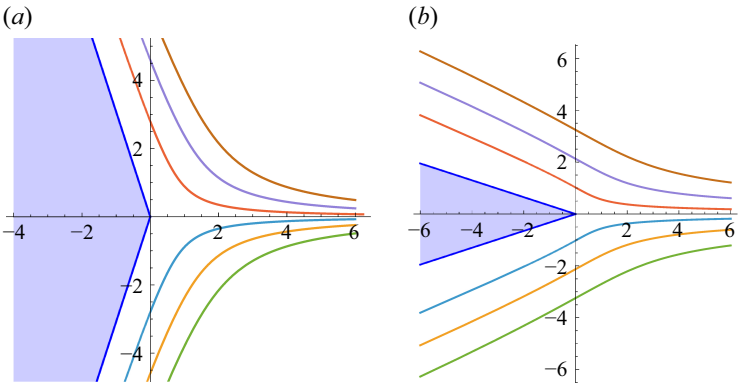


Figure 8. Streamlines $\psi = \text{const.}$ for (*a*) $\alpha = 0.6\,\pi$ and (*b*) $\alpha = 0.9\,\pi$. When the flow is directed from the right towards the vertex, the divergence of the streamlines indicates Lagrangian retardation of fluid particles.

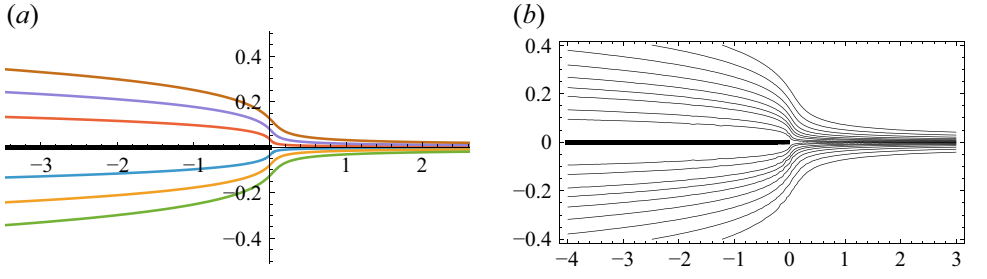


Figure 9. (*a*) Streamlines $\psi \propto r^{3/2}(1+\cos\theta)\sin(\theta/2) = \text{const.}$ in the limiting situation $\alpha = \pi$; (*b*) more detailed contour plot of streamlines from the equivalent Cartesian form, $\psi \propto [(x^2+y^2)^{1/2}+x]^{1/2}y$.

$$g(\theta, \alpha_c) \approx -\frac{1}{2}[\theta/\alpha_c + \sin 2\theta], \qquad \{-\alpha_c < \theta < \alpha_c\}. \tag{3.6}$$

Streamlines $\psi = \text{const.}$ for the cases $\alpha/\pi = 0.6$ and 0.9 are shown in figure 8(*a*,*b*). These are plotted using (3.1) (and (3.3) for $\mu(\alpha)$). In both cases it may be noted that the streamlines diverge approaching the vertex from the right, indicating (as might be expected in this case) deceleration of fluid particles on each streamline. (Again, arrows are not included on the streamlines, as the flows are in all cases reversible.)

Finally, figure 9(*a*) shows the limiting situation $\alpha = \pi$, $\mu(\alpha) = 1/2$; in this case, the limiting form of the streamfunction is

$$\psi(r, \theta) = r^{3/2} g(\theta, \pi) \sim -r^{3/2}(1+\cos\theta)\sin(\theta/2), \tag{3.7}$$

a solution of the Stokes equation originally identified by Carrier & Lin (1948) in their study of the boundary-layer flow on a flat plate. The equivalent Cartesian streamfunction is

$$\psi(x, y) \sim -\big[(x^2+y^2)^{1/2}+x\big]^{1/2} y, \tag{3.8}$$

with contour plot showing essentially the same streamlines in greater detail in figure 9(*b*).

4. Asymmetric flow in the flat-plate limit $\alpha = \pi$

The relevant roots $\mu_1(\alpha)$ and $\mu_2(\alpha)$ for the two cases of antisymmetric and symmetric flow are replicated again in figure 10, showing that $\mu_1(\alpha) \le \mu_2(\alpha)$ with equality only in

https://doi.org/10.1017/jfm.2026.12016 Published online by Cambridge University Press

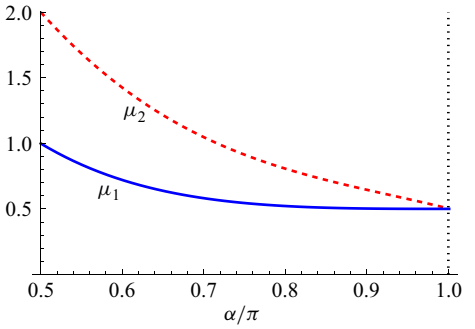


Figure 10. The functions $\mu_1(\alpha)$ and $\mu_2(\alpha)$ satisfying $F(\mu, \alpha) = 0$ and $G(\mu, \alpha) = 0$ respectively, showing that $\mu_1(\alpha) \leq \mu_2(\alpha)$, with equality only at the limit $\alpha = \pi$.

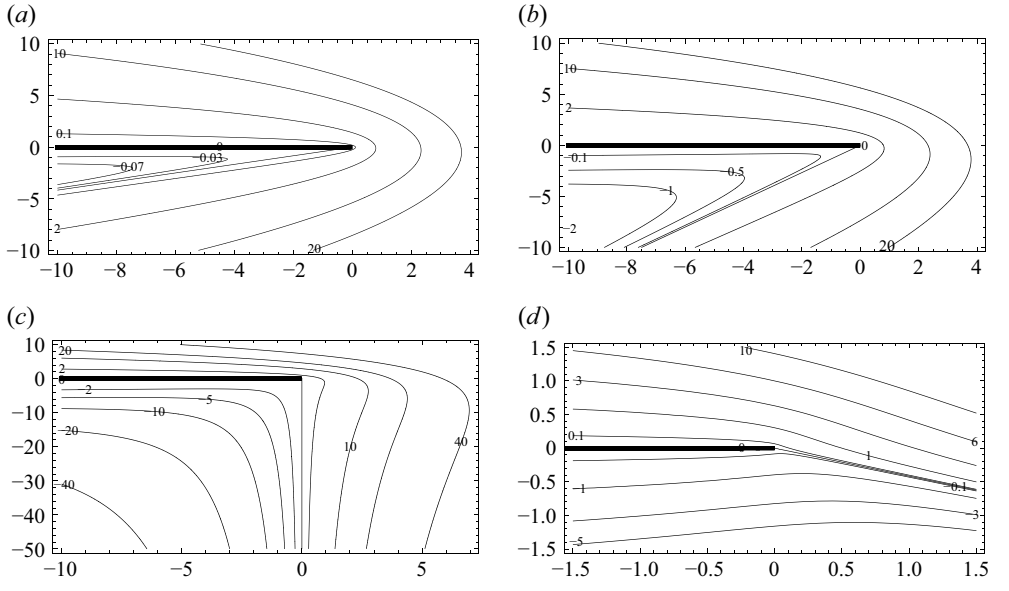


Figure 11. Streamlines $\psi = \psi_0$ for the streamfunction (4.1), with values of the constant ψ_0 on each streamline as marked; (*a*) $k = 0.2$; (*b*) $k = 0.5$; (*c*) $k = 1.0$; (*d*) $k = 5.0$.

the limiting flat-plate situation $\alpha = \pi$. In this limiting situation, any linear combination of the two flows (2.13) and (3.7) is a possible limiting solution of the Stokes equation $\nabla^4\psi = 0$ satisfying the no-slip conditions on both sides of the plate $\theta = \pm\pi$. In Cartesian coordinates, such a linear combination may be written as an expression, homogeneous in $\{x, y\}$ of degree $3/2$

$$\psi(x, y; k) = \left[(x^2 + y^2)^{1/2} + x\right]^{1/2}\left[(x^2 + y^2)^{1/2} + x + ky\right], \tag{4.1}$$

for arbitrary constant k. With this choice, note the obvious symmetry $\psi(x, y; -k) = \psi(x, -y; k)$.

Four sets of streamlines $\psi(x, y; k) = \text{const.}$ are shown in figure 11, for $k = 0.2$, 0.5, 1.0 and 5.0. These are the asymptotic forms of flow near the leading edge of the plate, where the parameter k is determined by remote conditions. Note how the separating streamline

https://doi.org/10.1017/jfm.2026.12016 Published online by Cambridge University Press

$\psi = 0$ rotates anticlockwise as k increases, asymptoting to $\theta = 0$ for large k (as in figure 9), when the rotating contribution to (4.1) is relatively weak.

5. Conclusions

(i) In § 2, flow round the corner of a wedge has been re-examined, and the acceleration of fluid particles as they approach the vicinity of the point of zero velocity at the tip of the corner has been noted and explained. In the limit $\alpha = \pi$ when the wedge collapses to a flat plate, the streamlines have been shown to be a family of parabolas.

(ii) In § 3, symmetric flow towards or away from the tip of a wedge has been similarly examined, and a critical point of the exponent function $\mu(\alpha)$ at $\alpha = \alpha_c \approx 0.715\pi$ has been identified (see figure 6). A family of solutions for the streamfunction, continuous through the critical point, has nevertheless been found and streamlines plotted for various values of α. The limiting solution for $\alpha = \pi$ is that first identified by Carrier & Lin (1948).

(iii) In § 4, it is shown that, in the flat-plate limit $\alpha = \pi$, symmetric and antisymmetric solutions may be combined to provide a family of asymptotic solutions with streamlines impinging at an arbitrary angle on the edge of the plate.

Acknowledgements. I am grateful to three referees whose helpful comments have led to significant improvements in this paper. I thank also Professor J. Rallison who, some 50 years ago, expressed doubts concerning the plausibility of figure 4(*a*) of Moffatt (1964).

Declaration of interests. The author declares no conflict of interest.

References

Bradley, M. 2015 Demonstrations.wolfram.com/FluidFlowAroundACorner/ *Wolfram demonstration project*. Wolfram.

Carrier, G.F. & Lin, C.C. 1948 On the nature of the boundary layer near the leading edge of a flat plate. *Q. Appl. Maths* **6** (1), 63–68.

Dean, W.R. & Montagnon, P.E. 1949 On the steady motion of viscous liquid in a corner. *Math. Proc. Camb. Phil. Soc.* **45** (3), 389–394.

Moffatt, H.K. 1964 Viscous and resistive eddies near a sharp corner. *J. Fluid Mech.* **18**, 1–18.

Moffatt, H.K. & Duffy, B.R. 1980 Local similarity solutions and their limitations. *J. Fluid Mech.* **96** (2), 299–313.

Shankar, P.N. 2007 *Slow Viscous Flows: Qualitative Features and Quantitative Analysis Using Complex Eigenfunction Expansions*. World Scientific.

Taneda, S. 1979 Visualization of separating Stokes flows. *J. Phys. Soc. Japan* **46** (6), 1935–1942.

https://doi.org/10.1017/jfm.2026.12016 Published online by Cambridge University Press